

Influence of Al₂O₃ content on mechanical properties of silica-based ceramic cores prepared by stereolithography

Wen ZHENG^{a,b}, Jia-Min WU^{a,b,*}, Shuang CHEN^{a,b}, Chang-Shun WANG^{a,b},
Chun-Lei LIU^{a,b}, Shuai-Bin HUA^{a,b}, Kang-Bo YU^{a,b}, Jie ZHANG^{a,b},
Jing-Xian ZHANG^c, Yu-Sheng SHI^{a,b,*}

^aState Key Laboratory of Materials Processing and Die & Mould Technology, School of Materials Science and Engineering, Huazhong University of Science and Technology, Wuhan 430074, China

^bEngineering Research Center of Ceramic Materials for Additive Manufacturing, Ministry of Education, Wuhan 430074, China

^cState Key Laboratory of High Performance Ceramics and Superfine Microstructure, Shanghai Institute of Ceramics, Chinese Academy of Sciences, Shanghai 200050, China

Received: April 21, 2021; Revised: June 10, 2021; Accepted: June 26, 2021

© The Author(s) 2021.

Abstract: Silica ceramic cores have played an important part in the manufacture of hollow blades due to their excellent chemical stability and moderate high-temperature mechanical properties. In this study, silica-based ceramics were prepared with Al₂O₃ addition by stereolithography, and the influence of Al₂O₃ content on mechanical properties of the silica-based ceramics was investigated. The Al₂O₃ in silica-based ceramics can improve the mechanical properties by playing a role as a seed for the crystallization of fused silica into cristobalite. As a result, with the increase of Al₂O₃ content, the linear shrinkage of the silica-based ceramics first decreased and then increased, while the room-temperature flexural strength and the high-temperature flexural strength first increased and then decreased. As the Al₂O₃ content increased to 1.0 vol%, the linear shrinkage was reduced to 1.64% because of the blocked viscous flow caused by Al₂O₃. Meanwhile, the room-temperature flexural strength and the high-temperature flexural strength were improved to 20.38 and 21.43 MPa with 1.0 vol% Al₂O₃, respectively, due to the increased α -cristobalite and β -cristobalite content. Therefore, using the optimal content of Al₂O₃ in silica-based ceramics can provide excellent mechanical properties, which are suitable for the application of ceramic cores in the manufacturing of hollow blades.

Keywords: silica; ceramic core; stereolithography; Al₂O₃; mechanical properties; hollow blades

1 Introduction

Silica-based ceramic cores with excellent thermal stability

* Corresponding authors.

E-mail: J.-M. Wu, jiaminwu@hust.edu.cn;
Y.-S. Shi, shiyusheng@hust.edu.cn

and good core leach have been widely used to fabricate the cavities of turbine engines and gas turbine hollow blades that require high precision and complex shapes [1–5]. However, the traditional preparation method based on investment casting has great limitations in the fabrication process. It not only requires a long production cycle, but also consumes expensive manufacturing costs,

which will limit the application and development of silica ceramic cores [6–8]. In order to deal with these problems relevant to the forming of complicated ceramic parts, a new advanced manufacturing technology—3D printing technology has been developed [9–12]. Compared with other ceramic 3D printing technologies, stereolithography possesses higher forming precision and better surface quality. The technology can use the laser beam to cure ceramic slurry layer by layer and obtain ceramic parts with complex structure by debinding and sintering process [13–17].

The forming process, sintering process, and raw materials have a great influence on the microstructure and mechanical properties of 3D-printed silica ceramics, whereas cracks often appear in the sintering stage because of shrinkage and phase transformation. Li *et al.* [18] investigated the effects of sintering temperatures on the mechanical properties of 3D-printed silica ceramic cores based on stereolithography. The room-temperature flexural strength of silica ceramic cores reached a maximum value of 12.1 MPa at the sintering temperature of 1300 °C. Kotz *et al.* [19] realized the significance of raw materials for preparing high-quality fused silica glass. They could create arbitrary macro- and microstructures from photocurable silica nanocomposites, thereby broadening the selection of 3D printing materials. Cai *et al.* [20] pointed out the influence of solid loading and mixing methods on silica glass fabricated by digital light processing (DLP). Their experimental data showed that the viscosity of slurry could be reduced effectively by the multi-step mixing method compared with the one-step mixing method. Liu *et al.* [21] noticed the efficiency problem of fabricating silica glass by stereolithography, thus developing a stereolithography system using top-down method and obtaining the glassware with similar properties to fused silica.

Although stereolithography provides a practical technical way for the efficient and high-quality manufacturing of silica ceramic parts [22,23], there exist some research difficulties. Firstly, the forming mode of layer-by-layer curing can easily cause larger linear shrinkage [24], which will not only affect the mechanical properties of ceramic parts, but also limit the wide application of ceramic products [25,26]. Secondly, 3D-printed silica ceramics show lower flexural strength. In addition, the high-temperature strength and room-temperature strength of 3D-printed silica ceramics are rarely investigated at the same time, which may

have a strong influence on the performance of ceramic cores. At present, the reinforcements in silica ceramics, such as cristobalite [27] or silicon carbide [4], can improve the mechanical properties effectively by promoting the development of cristobalite. Furthermore, Al₂O₃ has a fairly high flexural strength of 472 MPa [28] and thus contributes to enhancing the flexural strength of silica ceramics. Al₂O₃ can be also very helpful in reducing the shrinkage of silica ceramics by promoting the crystallization of the fused silica [29]. Therefore, the Al₂O₃ is promising to be regarded as a powerful reinforcement in silica ceramic cores.

In this work, silica-based ceramics added to various Al₂O₃ contents via stereolithography were fabricated. The influence of Al₂O₃ content on the mechanical properties of silica-based ceramics was investigated, and the room-temperature and the high-temperature mechanical properties of the as-obtained silica-based ceramics were both examined.

2 Materials and methods

2.1 Raw materials

The slurry used to prepare silica ceramics consisted of spherical SiO₂ powder (99.9% purity; Hebei Guihuang Metal Material Co., Ltd., China) with an average particle size of 2 μm, Al₂O₃ powder (purity 99.5%, average particle size 3 μm; Hebei Kegong Metallurgical Materials Co., Ltd., China), photosensitive resin HDDA (Shanghai Guangyi Chemical Co., Ltd., China), polymer dispersant 41000 (3 wt% of the SiO₂ powder; Lubrizol Advanced Materials S.L., Spain), and photoinitiator diphenyl (2,4,6-trimethylbenzoyl) phosphine oxide (TPO, 0.5 wt% of photosensitive resin; BASF, Germany). All ceramic powders and auxiliaries are commercially available. Meanwhile, the particle size distribution of raw powders is shown in Fig. 1, indicating the uniformity

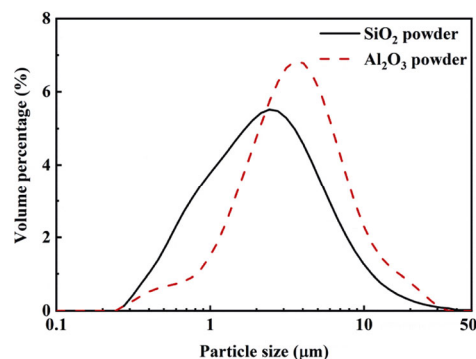


Fig. 1 Particle size distribution of raw powders.

of the particle size distribution of the raw powders.

2.2 Sample preparation

The solid loading of each ceramic slurry was set to 45 vol%. To match with the solid loading, the Al₂O₃ contents of the ceramic powders were 0, 0.5, 1.0, 1.5, and 2.0 vol%. When weighing Al₂O₃ in the preparation of the slurry, the corresponding mass was converted according to the density of 4.0 g/cm³ provided by the powder manufacturer, and then the composite powders were ball-milled in vacuum. The ceramic slurries were obtained by milling the mixture about 30 min at room temperature. Table 1 shows the viscosity of the slurries with different contents of Al₂O₃ at the same shear rate of 50 s⁻¹. As a result, all the slurries had good liquidity that the viscosity of them was less than 10 Pa·s, which is suitable for forming by stereolithography [30,31]. After obtaining the slurries, the green bodies were formed by a 3D printer (Wuhan Intelligent Laser Technology Co., Ltd., China). And the sizes of the ceramic green bodies used to test flexural strength were 60 mm × 5 mm × 3.6 mm (*L* × *W* × *H*). In this 3D printing mode, the *z*-axis displacement distance of the 3D printer for the green bodies was set to 3.6 mm. With the process parameters optimized, the laser power was 0.75 W, the scanning speed was 3000 mm/s, and the thickness of each layer was 50 μm.

A thermogravimetric analyzer (TGA; PerkinElmer Instrument (Shanghai) Co., Ltd., China) was used to analyze the powder ground from green bodies. The thermogravimetric curve shown in Fig. 2(a) was obtained, and the optimal debinding and sintering process could be determined from the curve analysis. As shown in Fig. 2(b), the resin could be completely removed by holding at 600 °C for 2 h. Sintered at 1200 °C for about 6 h, silica-based ceramic samples could achieve a higher degree of densification.

2.3 Characterization

The particle size distribution was measured by a laser

Table 1 Viscosity of the slurries with different contents of Al₂O₃

Al ₂ O ₃ content (vol%)	Viscosity (Pa·s)
0	7.66
0.5	3.22
1.0	4.93
1.5	3.74
2.0	8.65

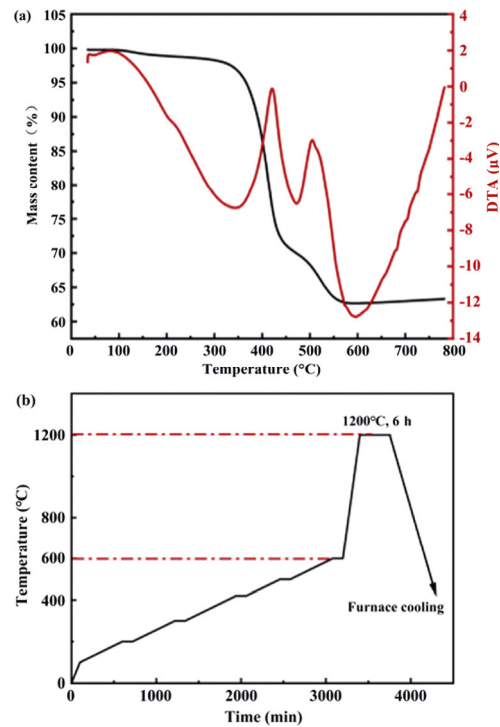


Fig. 2 Thermogravimetric curve and thermal treatment of SiO₂ green bodies: (a) TG–DTA curve and (b) debinding and sintering curve.

diffraction particle size analyzer (Mastersizer 3000, UK). The phase transformations of ceramic samples were detected by an X-ray diffractometer (XRD-6100, Shimadzu, Japan). Meanwhile, scanning electron microscopy (SEM) images were observed by field-emission SEM (Quanta650 FEG, FEI, USA). The bulk density and apparent porosity of the silica-based ceramics were measured by the Archimedes principle [32]. To measure the flexural strength of the silica-based ceramic samples at room temperature, an electronic universal testing machine (E1000, ITW Group Instron Inc., USA) was used. The span was adjusted to 30 mm, and the loading rate was set to 0.5 mm/min. Five samples fabricated with each Al₂O₃ content were tested, and the average value was taken as the reference value of the room-temperature flexural strength. Moreover, the high-temperature strength was measured with a heating rate of 5 °C/min up to 1550 °C, using a ceramic flexural strength tester (WDW-20, Shenyang Foundry Research Institute Co., Ltd., China). Test methods were performed consistent with the standard HB5352.1-2004. The formula adopted to calculate the flexural strength (σ) is as follows:

$$\sigma = \frac{3FL}{2bh^2} \tag{1}$$

where *F* is the load when the test sample is broken, *L* is

the span between the two fulcrums, b is the width of the test sample, and h is the thickness of the test sample.

3 Results and discussion

The phase compositions of silica-based ceramics with various Al_2O_3 contents are gathered in Fig. 3. All sintered ceramics contain quartz resulting from the crystallization of the fused silica. The fused silica has crystallized into quartz at the sintering temperature of $1200\text{ }^\circ\text{C}$ [33]. On the XRD patterns, the peak of the Al_2O_3 pattern is not very evident due to its low content. Meanwhile, the cristobalite peaks located at about 21.80° are detected in all-ceramic samples that contain Al_2O_3 (0.5, 1.0, 1.5, and 2.0 vol%), and the intensity increases with the increase of Al_2O_3 content, indicating that Al_2O_3 can contribute to the formation of cristobalite and its relative content is correlated positively with the Al_2O_3 content. However, the cristobalite peaks are not detected in the ceramic samples without Al_2O_3 . The XRD results suggest that the fused silica crystallizes into cristobalite due to the emergence of Al_2O_3 . And the generated cristobalite is conducive to the mechanical properties of silica ceramics. Therefore, Al_2O_3 can improve the mechanical properties of silica-based ceramics by accelerating the crystallization of the fused silica.

The microstructures of silica-based ceramics prepared with various contents of Al_2O_3 are shown in Fig. 4. Large grains and pores appear in sintered ceramics

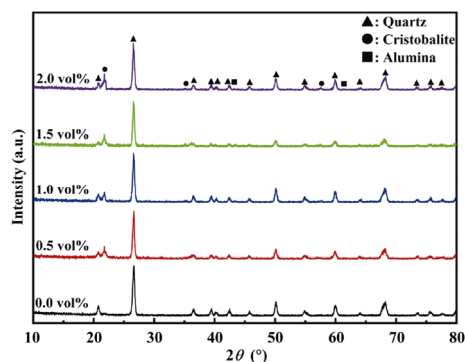


Fig. 3 XRD patterns of silica-based ceramic samples with different contents of Al_2O_3 .

regardless of the Al_2O_3 content. To explore the elemental composition of the sintered ceramics, the ceramic samples sintered at $1200\text{ }^\circ\text{C}$ are observed by energy dispersive X-ray spectroscopy (EDS) and the data are obtained. As shown in Fig. 4(f), the Al and Si elements are both found in the ceramic samples containing 1.5 vol% Al_2O_3 . Meanwhile, plenty of SiO_2 crystals with 3D network structure can be seen because the crystallization temperature of the fused silica is less than $1200\text{ }^\circ\text{C}$ [34]. In the fracture of the silica ceramic without adding Al_2O_3 , the grains are tightly bonded. After adding Al_2O_3 , there are more pores in silica-based ceramics containing 0.5 and 1.0 vol% Al_2O_3 than that without Al_2O_3 . Thus it can be seen that Al_2O_3 has some inhibitory effects on the binding between grains. As the Al_2O_3 increases to 1.5 and 2.0 vol%, the ceramic grains grow coarsely, weakening the inhibitory effect to a certain extent.

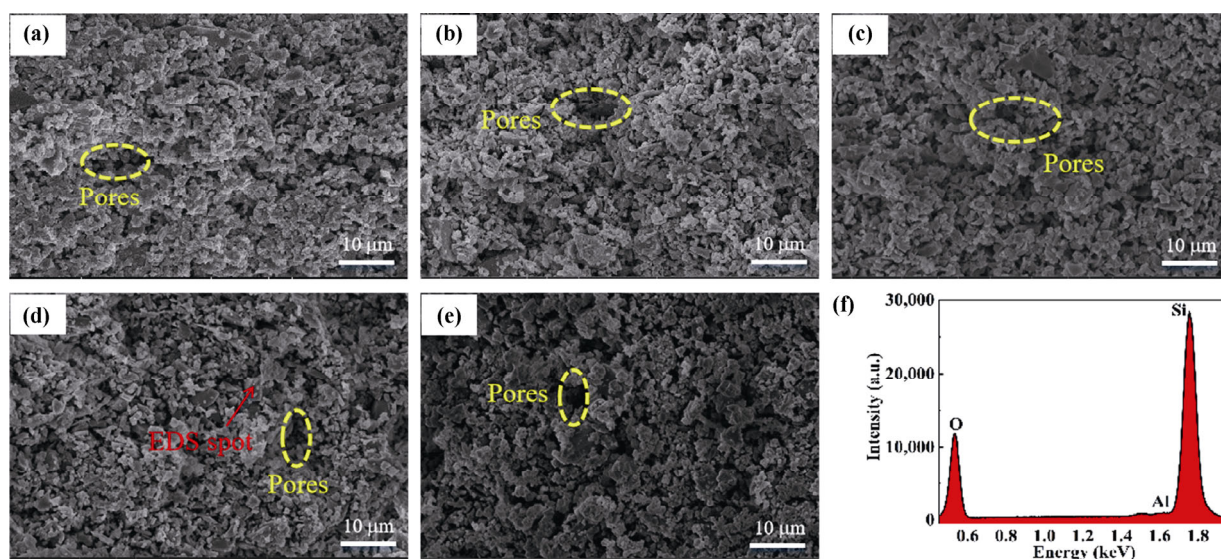


Fig. 4 Microstructures of the silica-based ceramics with various contents of Al_2O_3 : (a) 0, (b) 0.5, (c) 1.0, (d) 1.5, (e) 2.0 vol%, and (f) EDS analysis of the EDS spot with 1.5 vol% Al_2O_3 .

As shown in Fig. 5(a), with the decrease of temperature during the cooling process, β -cristobalite gradually transforms into α -cristobalite in turn, demonstrating the existence of the phase transformation in the silica-based ceramics. Meanwhile, mullite is formed because of the reaction between quartz and Al_2O_3 at the high temperature of $1550\text{ }^\circ\text{C}$, as presented in Eq. (2). In addition, the silica-based ceramics measured at $1550\text{ }^\circ\text{C}$ with 1.0 vol% Al_2O_3 generate liquid phase, as presented in Fig. 5(b), which is absent under the sintering temperature of $1200\text{ }^\circ\text{C}$, as suggested in Fig. 4. The liquid phase is generated by the melting silica at high temperatures, connecting interlayer independent grains [18], as well as increasing the adhesion between ceramic grains and contributing to improved mechanical properties of silica-based ceramics. Furthermore, visible cracks appear in the silica-based ceramics measured at $1550\text{ }^\circ\text{C}$ due to the phase transformation from α -cristobalite to stable β -cristobalite during the thermal treatment process.

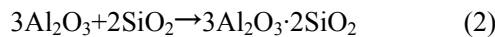


Figure 6(a) shows the linear shrinkage of silica-based ceramics with different contents of Al_2O_3 . The linear shrinkage of the samples is reduced from 2.62% to 1.64% as the Al_2O_3 increases to 1.0 vol%. The crystalline phases in the silica-based ceramics, such as Al_2O_3 and

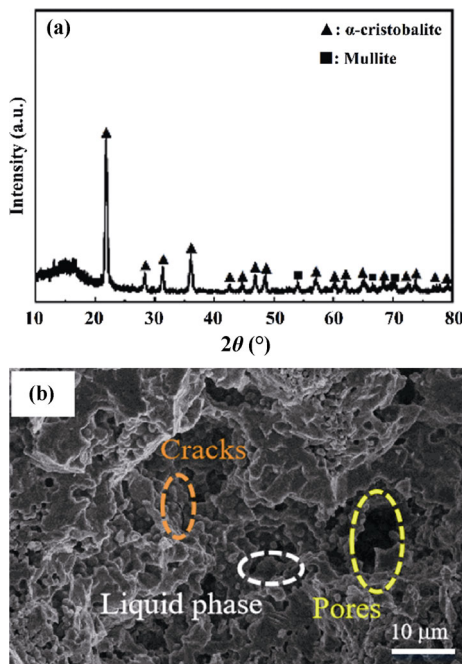


Fig. 5 (a) XRD pattern and (b) SEM image of the silica-based ceramics measured at $1550\text{ }^\circ\text{C}$ with 1.0 vol% Al_2O_3 .

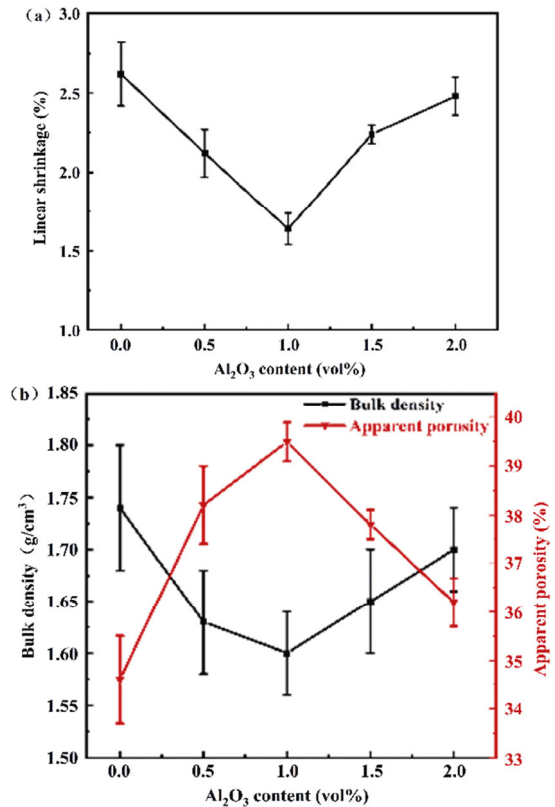


Fig. 6 (a) Linear shrinkage and (b) bulk density and apparent porosity of silica-based ceramics with different contents of Al_2O_3 .

cristobalite, can promote the crystallization of the fused silica, but cause relatively small shrinkage. Additionally, the crystalline phases also hinder the viscous flow that is the driving force of the densification of the fused silica, which becomes an obstacle to the shrinkage [35,36]. Consequently, the addition of Al_2O_3 degrades the linear shrinkage of the silica-based ceramics. Nevertheless, the linear shrinkage is upgraded to 2.52% with excessive Al_2O_3 (1.5 and 2.0 vol%), which is still lower than the silica ceramics without Al_2O_3 . When the Al_2O_3 content increases to 2.0 vol%, the Al_2O_3 improves the densification of the ceramics by promoting the growth of coarse grains, as shown in Fig. 4. The improvement has nullified part of the weakening effect caused by the crystalline phases, bringing about the increased linear shrinkage of the silica-based ceramics.

The bulk density and the apparent porosity results of the silica-based ceramics sintered at $1200\text{ }^\circ\text{C}$ are shown in Fig. 6(b). When the Al_2O_3 increases from 0 to 1.0 vol%, the fused silica is transformed into β -cristobalite with cubic structure during high-temperature sintering due to the emergence of Al_2O_3 . Meanwhile, around $250\text{ }^\circ\text{C}$ in the cooling course, the phase transition from

β -cristobalite to α -cristobalite with tetragonal structure is realized [37,38]. The phase transition will bring a 5% reduction of volume, which is likely to cause the propagation of microcracks in silica ceramics [38,39]. Under the combined effect of phase transition and crystallization, the apparent porosity increases and the bulk density decreases. With Al_2O_3 added to 2.0 vol%, the ceramic grains grow coarsely due to the effect of mass transfer between phases induced by Al_2O_3 . The volume change resulting from coarse grains can improve the densification of silica-based ceramics. At this moment, the improvement of the densification overcomes the weakening effect of phase transition, which leads to the decrease of the apparent porosity and the increase of the bulk density.

The flexural strength of the silica-based ceramics prepared from green bodies with various contents of Al_2O_3 printed by the 3D printer is presented in Fig. 7. It is indicated that the flexural strength of the ceramics all shows an opposite tendency to the linear shrinkage. The room-temperature flexural strength of the ceramic samples is improved from 11.56 to 20.38 MPa as the Al_2O_3 increases to 1.0 vol%. Compared with the amorphous silica, cristobalite has a higher strength. Therefore, the crystallization of the fused silica into cristobalite can improve the room-temperature flexural strength of the silica ceramics [40,41]. However, the room-temperature flexural strength of the samples decreases when the Al_2O_3 increases to 1.5 and 2.0 vol%. Although cristobalite provides silica-based ceramics with better strength, excessive cristobalite may weaken the trend in turn. The flexural strength of the fused silica ceramics will decrease when the generation of cristobalite is more than 30% [40]. In this study, it seems easier for the fused silica added Al_2O_3 to crystallize into α -cristobalite. As a result, the room-temperature flexural strength is enhanced as the Al_2O_3 increases to 1.0 vol%. But excessive Al_2O_3 (1.5 and 2.0 vol%) reduces the internal binding force by accelerating the nucleation of the crystallization process, thereby degrading the flexural strength. Furthermore, both the flexural strength and the apparent porosity of the silica-based ceramics increase as the Al_2O_3 increases to 1.0 vol%. Although the volume reduction brought by the phase transition is disadvantageous to the strength, the enhancement of cristobalite induced by Al_2O_3 is much stronger than the weakening effect. Thus, the flexural strength of the silica-based ceramics is also improved with the increase of the apparent porosity.

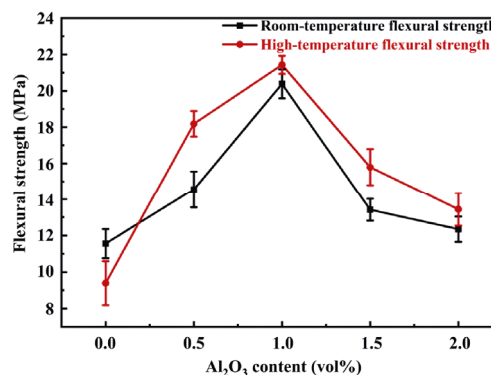


Fig. 7 Flexural strength of silica-based ceramics with different contents of Al_2O_3 .

As for the high-temperature flexural strength, it is improved from 9.39 to 21.43 MPa as the Al_2O_3 increases to 1.0 vol%, but excessive Al_2O_3 (1.5 and 2.0 vol%) reduces the strength. Obviously, the trend is similar to the flexural strength at room temperature. What's more, there are some different degrees of improvement compared with the room-temperature flexural strength under the same content of Al_2O_3 . The surface of the fused silica grains will spontaneously separate stable β -cristobalite crystals out at high temperature [42,43], thus improving the high-temperature strength of silica-based ceramics. However, when the content of β -cristobalite is too high, the volume effect caused by the secondary crystal transformation of cristobalite produces more microcracks inside the silica ceramics, reducing the high-temperature flexural strength. Arguably, the β -cristobalite generated under the high temperature of 1550 °C is highly responsible for improving the high-temperature flexural strength of silica-based ceramics due to its high strength.

4 Conclusions

In this study, the silica-based green bodies were fabricated via stereolithography, and the influence of Al_2O_3 content on mechanical properties and microstructures of the as-sintered silica-based ceramics was systematically investigated. With the increase of Al_2O_3 content, the linear shrinkage of the sintered ceramics first decreased and then increased, while the room-temperature flexural strength and the high-temperature flexural strength first increased and then decreased. With Al_2O_3 added to 1.0 vol%, the linear shrinkage reached 1.64% due to the blocked viscous flow. Nevertheless, the excessive Al_2O_3 (1.5 and 2.0 vol%) could increase the linear

shrinkage by promoting the growth of coarse grains which can improve the densification of silica-based ceramics. The Al₂O₃ in the silica-based ceramics served as a seed for the crystallization of the fused silica into cristobalite, thereby improving the mechanical properties. Therefore, the room-temperature flexural strength was enhanced to 20.38 MPa and the high-temperature flexural strength was improved to 21.43 MPa, as the Al₂O₃ content increased to 1.0 vol%. However, a large amount of cristobalite generated by the high content of Al₂O₃ could easily reduce the internal binding force and cause the propagation of microcracks inside the silica-based ceramics, thus degrading the room-temperature flexural strength and the high-temperature flexural strength. All in all, the results suggest that using the optimal content of Al₂O₃ provides optimum mechanical properties, which are appropriate for the wide application of silica-based ceramic cores and contribute to the manufacturing of hollow blades.

Acknowledgements

The research work presented in this paper is supported by the National Science and Technology Major Project (2017-VII-0008-0102), the National Natural Science Foundation of China (51975230), and the Opening Project of State Key Laboratory of High Performance Ceramics and Superfine Microstructure (SKL201903SIC). Meanwhile, the authors are grateful for the State Key Laboratory of Materials Processing and Die & Mould Technology for mechanical property tests, as well as the Analysis and Testing Center of Huazhong University of Science and Technology for XRD and SEM tests.

References

- [1] Zhong JW, Xu QY. High-temperature mechanical behaviors of SiO₂-based ceramic core for directional solidification of turbine blades. *Materials* 2020, **13**: 4579.
- [2] Bae CJ, Kim D, Halloran JW. Mechanical and kinetic studies on the refractory fused silica of integrally cored ceramic mold fabricated by additive manufacturing. *J Eur Ceram Soc* 2019, **39**: 618–623.
- [3] Huseby IC, Borom MP, Greskovich CD. High temperature characterization of silica-base cores for superalloys. *Am Ceram Soc Bull* 1979, **58**: 448–452.
- [4] Kim YH, Yeo JG, Lee JS, *et al.* Influence of silicon carbide as a mineralizer on mechanical and thermal properties of silica-based ceramic cores. *Ceram Int* 2016, **42**: 14738–14742.
- [5] Kim YH, Yeo JG, Choi SC. Shrinkage and flexural strength improvement of silica-based composites for ceramic cores by colloidal alumina infiltration. *Ceram Int* 2016, **42**: 8878–8883.
- [6] Chen X, Zheng WL, Zhang J, *et al.* Enhanced thermal properties of silica-based ceramic cores prepared by coating alumina/mullite on the surface of fused silica powders. *Ceram Int* 2020, **46**: 11819–11827.
- [7] He X, Ding YC, Lei ZP, *et al.* 3D printing of continuous fiber-reinforced thermoset composites. *Addit Manuf* 2021, **40**: 101921.
- [8] Chen ZW, Li ZY, Li JJ, *et al.* 3D printing of ceramics: A review. *J Eur Ceram Soc* 2019, **39**: 661–687.
- [9] Chen Z, Sun XH, Shang YP, *et al.* Dense ceramics with complex shape fabricated by 3D printing: A review. *J Adv Ceram* 2021, **10**: 195–218.
- [10] Li H, Liu YS, Liu YS, *et al.* Effect of sintering temperature in argon atmosphere on microstructure and properties of 3D printed alumina ceramic cores. *J Adv Ceram* 2020, **9**: 220–231.
- [11] Liu SS, Li M, Wu JM, *et al.* Preparation of high-porosity Al₂O₃ ceramic foams via selective laser sintering of Al₂O₃ poly-hollow microspheres. *Ceram Int* 2020, **46**: 4240–4247.
- [12] Yao YX, Qin W, Xing BH, *et al.* High performance hydroxyapatite ceramics and a triply periodic minimum surface structure fabricated by digital light processing 3D printing. *J Adv Ceram* 2021, **10**: 39–48.
- [13] Feng CW, Zhang KQ, He RJ, *et al.* Additive manufacturing of hydroxyapatite bioceramic scaffolds: Dispersion, digital light processing, sintering, mechanical properties, and biocompatibility. *J Adv Ceram* 2020, **9**: 360–373.
- [14] Ding GJ, He RJ, Zhang KQ, *et al.* Stereolithography 3D printing of SiC ceramic with potential for lightweight optical mirror. *Ceram Int* 2020, **46**: 18785–18790.
- [15] Grigoryan B, Sazer DW, Avila A, *et al.* Development, characterization, and applications of multi-material stereolithography bioprinting. *Sci Rep* 2021, **11**: 3171.
- [16] Chen F, Zhu H, Wu JM, *et al.* Preparation and biological evaluation of ZrO₂ all-ceramic teeth by DLP technology. *Ceram Int* 2020, **46**: 11268–11274.
- [17] Kozlov DA, Tikhonova SA, Evdokimov PV, *et al.* Stereolithography 3D printing from suspensions containing titanium dioxide. *Russ J Inorg Chem* 2020, **65**: 1958–1964.
- [18] Li H, Hu KH, Liu YS, *et al.* Improved mechanical properties of silica ceramic cores prepared by 3D printing and sintering processes. *Scripta Mater* 2021, **194**: 113665.
- [19] Kotz F, Arnold K, Bauer W, *et al.* Three-dimensional printing of transparent fused silica glass. *Nature* 2017, **544**: 337–339.
- [20] Cai P, Guo L, Wang H, *et al.* Effects of slurry mixing methods and solid loading on 3D printed silica glass parts based on DLP stereolithography. *Ceram Int* 2020, **46**: 16833–16841.
- [21] Liu C, Qian B, Liu XF, *et al.* Additive manufacturing of silica glass using laser stereolithography with a top-down approach

- and fast debinding. *RSC Adv* 2018, **8**: 16344–16348.
- [22] Ji SH, Kim DS, Park MS, *et al.* Sintering process optimization for 3YSZ ceramic 3D-printed objects manufactured by stereolithography. *Nanomaterials* 2021, **11**: 192.
- [23] Mukhtarkhanov M, Perveen A, Talamona D. Application of stereolithography based 3D printing technology in investment casting. *Micromachines* 2020, **11**: 946.
- [24] Manière C, Kerbart G, Harnois C, *et al.* Modeling sintering anisotropy in ceramic stereolithography of silica. *Acta Mater* 2020, **182**: 163–171.
- [25] Liu J, Wang QH, Li YW, *et al.* Inhibiting crystallization of fused silica ceramic at high temperature with addition of α -Si₃N₄. *Ceram Int* 2021, **47**: 11394–11404.
- [26] Wang YY, Li L, Wang ZY, *et al.* Fabrication of dense silica ceramics through a stereo lithography-based additive manufacturing. *Solid State Phenom* 2018, **281**: 456–462.
- [27] Niu SX, Xu XQ, Li X, *et al.* Enhanced properties of silica-based ceramic cores by controlled particle sizes of cristobalite seeds. *Adv Appl Ceram* 2019, **118**: 403–408.
- [28] Wang JC. A novel fabrication method of high strength alumina ceramic parts based on solvent-based slurry stereolithography and sintering. *Int J Precis Eng Manuf* 2013, **14**: 485–491.
- [29] An GS, Choi SW, Kim YH, *et al.* Effective infiltration with polyethyleneimine-grafted colloidal alumina particles for silica-based ceramic cores. *J Ceram Soc Jpn* 2017, **125**: 95–99.
- [30] Goswami A, Ankit K, Balashanmugam N, *et al.* Optimization of rheological properties of photopolymerizable alumina suspensions for ceramic microstereolithography. *Ceram Int* 2014, **40**: 3655–3665.
- [31] Zhang S, Sha N, Zhao Z. Surface modification of α -Al₂O₃ with dicarboxylic acids for the preparation of UV-curable ceramic suspensions. *J Eur Ceram Soc* 2017, **37**: 1607–1616.
- [32] Chen X, Liu CY, Zheng WL, *et al.* High strength silica-based ceramics material for investment casting applications: Effects of adding nanosized alumina coatings. *Ceram Int* 2020, **46**: 196–203.
- [33] Kazemi A, Faghihi-Sani MA, Alizadeh HR. Investigation on cristobalite crystallization in silica-based ceramic cores for investment casting. *J Eur Ceram Soc* 2013, **33**: 3397–3402.
- [34] Huang LP, Duffrène L, Kieffer J. Structural transitions in silica glass: Thermo-mechanical anomalies and polyamorphism. *J Non-Cryst Solids* 2004, **349**: 1–9.
- [35] Sacks MD, Bozkurt N, Scheffele GW. Fabrication of mullite and mullite-matrix composites by transient viscous sintering of composite powders. *J Am Ceram Soc* 1991, **74**: 2428–2437.
- [36] Duan WJ, Yang ZH, Cai DL, *et al.* Effect of sintering temperature on microstructure and mechanical properties of boron nitride whisker reinforced fused silica composites. *Ceram Int* 2020, **46**: 5132–5140.
- [37] Kazemi A, Faghihi-Sani MA, Nayyeri MJ, *et al.* Effect of zircon content on chemical and mechanical behavior of silica-based ceramic cores. *Ceram Int* 2014, **40**: 1093–1098.
- [38] Breneman RC, Halloran JW. Effect of cristobalite on the strength of sintered fused silica above and below the cristobalite transformation. *J Am Ceram Soc* 2015, **98**: 1611–1617.
- [39] Peacor DR. High-temperature single-crystal study of the cristobalite inversion. *Zeitschrift Für Kristallographie* 1973, **138**: 274–298.
- [40] Xia GB, He L, Yang DA. Preparation and characterization of CaO–Al₂O₃–SiO₂ glass/fused silica composites for LTCC application. *J Alloys Compd* 2012, **531**: 70–76.
- [41] Yang ZG, Zhao ZJ, Yu JB, *et al.* Preparation of silica ceramic cores by the preceramic pyrolysis technology using silicone resin as precursor and binder. *Mater Chem Phys* 2019, **223**: 676–682.
- [42] Bae CJ. Integrally cored ceramic investment casting mold fabricated by ceramic stereolithography. Ph.D. Thesis. Ann Arbor, USA: University of Michigan, Ann Arbor, 2008.
- [43] Beeley PR, Smart RF. *Investment Casting*. London, UK: Cambridge University Press, 1995.

Open Access This article is licensed under a Creative Commons Attribution 4.0 International License, which permits use, sharing, adaptation, distribution and reproduction in any medium or format, as long as you give appropriate credit to the original author(s) and the source, provide a link to the Creative Commons licence, and indicate if changes were made.

The images or other third party material in this article are included in the article's Creative Commons licence, unless indicated otherwise in a credit line to the material. If material is not included in the article's Creative Commons licence and your intended use is not permitted by statutory regulation or exceeds the permitted use, you will need to obtain permission directly from the copyright holder.

To view a copy of this licence, visit <http://creativecommons.org/licenses/by/4.0/>.